

Mn(I)-catalyzed sigmatropic rearrangement of β , γ -unsaturated alcohols

Received: 8 July 2022

Accepted: 7 March 2023

Published online: 03 April 2023

Can Yang¹, Xiaoyu Zhou², Lixing Shen¹, Zhuofeng Ke²✉, Huanfeng Jiang¹ & Wei Zeng¹✉

Sigmatropic rearrangement provides a versatile strategy to site-selectively reorganize carbon-skeleton with high atom- and step-economy. Herein, we disclose a Mn(I)-catalyzed sigmatropic rearrangement of β , γ -unsaturated alcohols via C–C σ bond activation. A variety of α -aryl-allylic alcohols and α -aryl-propargyl alcohols could undergo in-situ 1,2- or 1,3- sigmatropic rearrangements to allow for converting to complex structural arylethyl- and arylvinyl-carbonyl compounds under a simple catalytic system. More importantly, this catalysis model can be further applied to assemble macrocyclic ketones through bimolecular $[2n + 4]$ coupling-cyclization and monomolecular $[n + 1]$ ring-extension. The presented skeleton rearrangement would be a useful tool complementary to the traditional molecular rearrangement.

Molecular rearrangements exist ubiquitously in modern synthetic chemistry, providing a powerful strategy to reorganize complex structures in an atom- and step-economic process through one-step chemical transformation^{1,2}. Almost a century ago, the Beckmann rearrangement^{3,4}, semi-pinacol rearrangement^{5–7}, Smiles rearrangement^{8–12}, Wolff rearrangement^{13–17}, and others¹⁸ have been successively developed to allow for diversified group migration via parallel moving pattern (Fig. 1a). Meanwhile, the Cope and Claisen rearrangement^{19–21} and Wittig rearrangement^{22,23} represent another type of cyclic transition state-based $[3,3]$ - and $[2,3]$ -sigmatropic shift, one of the most important features of these rearrangements involves synergetic C–X σ bond (X = C, O, N, etc.) formation and double-bond migration at pericyclic reaction-sites (Fig. 1b). To date, these classical group migratory and sigmatropic rearrangements have shown extremely potential in strategic synthesis of natural products, pharmaceuticals, and material molecules^{24–26}. However, it is surprising that 1,2-sigmatropic rearrangement (1,2-STR) or 1,3-sigmatropic rearrangement (1,3-STR), which only involves two different reaction-sites, has remained unexplored. This protocol will probably establish an efficient platform to enable in-situ U-turn-like rearrangement, which refers to a U-shaped turn made by a molecular skeleton so as to head in the opposite direction from its original course.

Although C–C σ bond activation belongs to a significantly challenging transformation due to the high C–C bond

dissociation energy and kinetical inertia^{27,28}, C–C σ bond functionalization has proven to be a straightforward approach to modifying complex carbon skeletons^{29–40}. Unfortunately, the current unstrained C–C σ bond activation strategies generally lead to the loss of another carbon-containing component derived from C–C bond cleavage^{28,33}. Thus, the development of unstrained C–C σ bond functionalization via rearrangement with high atomic and step-economy remains unmet challenges: (i) the efficient carbon-carbon activation-based group-switch generally requires 2–5 equivalents of coupling reagents^{36,37,39,40}, but the stoichiometric ratio of the cleaved moieties and the parent carbon skeletons is only up to a maximum of 1; (ii) the cleaved and lost carbon-containing moieties generally possess high reactivity and suffer from rapid decompositions either by processes of nucleophilic attack or by oxidation^{35–37}, leading to significant difficulty in their re-utilization. Nevertheless, given that ligand-directed C–C bond activation generally involves a cyclometalation process, which possibly once again traps the unsaturated carbonyl, vinyl or alkynyl species derived from C–C bond cleavage through the delicate balance between substrate-based reactivity and metal-based catalytical activity. Here, we show a Mn(I)-catalyzed carbon-skeleton reorganization of α -aryl- β , γ -unsaturated alcohols via C–C σ bond activation-based sigmatropic rearrangement (Fig. 1c).

¹Key Laboratory of Functional Molecular Engineering of Guangdong Province, School of Chemistry and Chemical Engineering, South China University of Technology, 510641 Guangzhou, China. ²School of Materials Science and Engineering, PFCM Lab, Sun Yat-sen University, 510275 Guangzhou, China.

✉ e-mail: kezhf3@mail.sysu.edu.cn; zengwei@scut.edu.cn

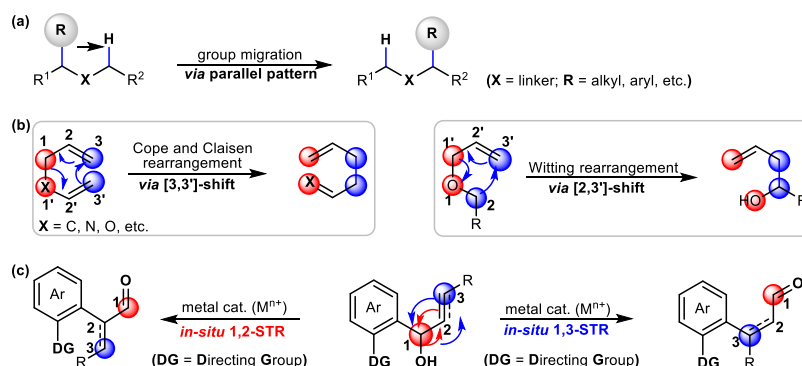


Fig. 1 | Strategies to access molecular skeleton rearrangement. **a** The traditional migratory patterns in Smiles, semi-pinacol, Beckmann, and Wolff rearrangements. **b** The sigmatropic shift in the Cope and Claisen rearrangement and the Wittig

rearrangement. **c** This work: Mn(I)-catalyzed 1,2-STR or 1,3-STR of α -aryl- β , γ -unsaturated alcohols.

Table 1 | Reaction development^a

Entry	Catalysts	Temperature (°C)	Solvents	Yield (2a/3a) (%) ^b
1	MnCl ₂	25	PhMe	0/0
2	Mn(OTf) ₂	25	PhMe	0/0
3	Mn(OAc) ₃ ·2H ₂ O	25	PhMe	0/0
4	Mn ₂ (CO) ₁₀	25	PhMe	0/23
5	Mn(CO) ₅ Br	25	PhMe	3/27
6	Mn(CO) ₅ Br	45	PhMe	4/56
7	Mn(CO) ₅ Br	75	PhMe	7/61
8	Mn(CO) ₅ Br	85	PhMe	5/54
9	Mn(CO) ₅ Br	75	PhCF ₃	0/43
10	Mn(CO) ₅ Br	75	THF	0/17
11	Mn(CO) ₅ Br	75	DMF	0/38
12	Mn(CO) ₅ Br	75	CH ₃ CN	0/0
13	Mn(CO) ₅ Br	75	DCE	0/80
14	Cp*Co(CO) ₂	75	DCE	0/5
15	Cp*Rh(CH ₃ CN) ₃ (SbF ₆) ₂	75	DCE	47/25

^aAll the reactions were performed using **1a** (0.20 mmol) and catalysts (0.01 mmol, 5 mol %) in solvent (2.0 mL) by heat for 24 h under Ar atmosphere in a sealed tube, followed by flash chromatography on SiO₂.

^bThe yields were determined by isolation.

Results

Investigation of reaction conditions

Earth-abundant first-row metal catalysts, which possess low cost, excellent sustainability, and environmentally benign properties, have attracted increasing attention in modern synthetic chemistry^{41–46}. Nevertheless, the exploration of non-noble-transition metal-catalyzed carbon-skeleton rearrangements is very scarce^{47,48}. The choice of Mn-catalysts was motivated by the notion that the valence electron configuration (3d⁵4s²) of elemental manganese endows different oxidation states of manganese species with distinctive coordination to arenes, alkenes, and alkynes^{49,50}. We therefore utilized 1-(1-(pyridin-2-yl)-1H-indol-2-yl)prop-2-en-1-ol (**1a**) as a model substrate to evaluate the feasibility of Mn-catalyzed [1,3]-sigmatropic rearrangement via carbon–carbon sigma bond activation (Table 1). First, various manganese salts such as Mn(OTf)₂, Mn₂(CO)₁₀, and Mn(CO)₅Br, etc. were

investigated in toluene to optimize the catalyst system (entries 1–5), we were quite pleased to find that the treatment of substrate **1a** with Mn₂(CO)₁₀ and Mn(CO)₅Br at room temperature (25 °C) did furnish 23% and 27% yield of 3-(1H-indol-2-yl)propanal **3a** (entries 4 and 5), respectively, in which the allylic-alcohol moiety of **1a** underwent a 1,3-STR through an in-situ carbon-skeleton-rearrangement; Meanwhile, 2-unsubstituted indole **2a**, which derived from the carbon–carbon bond cleavage and protonation, could also be obtained in 3% yield (entry 5). To our delight, after various reaction temperatures were scouted by employing Mn(CO)₅Br as catalysts (entries 5–8), it was found that running this transformation at 75 °C brought us increased conversion, affording 61% yield of 1,3-STR product **3a** and 7% yield of **2a** (entries 5–8 vs. 7). More satisfactorily, screening solvent systems further confirmed that 1,2-dichloroethane (DCE) showed a positive effect on this reaction, significantly increasing the reaction yield to

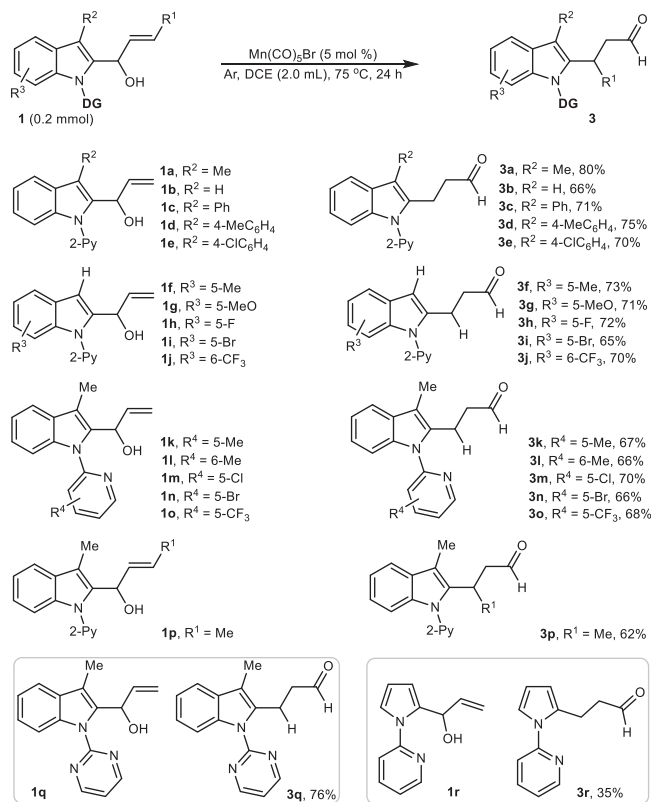


Fig. 2 | Secondary allylic-alcohol scope. All the reactions were performed in a sealed tube, followed by flash chromatography on SiO₂. The yields were determined by isolation.

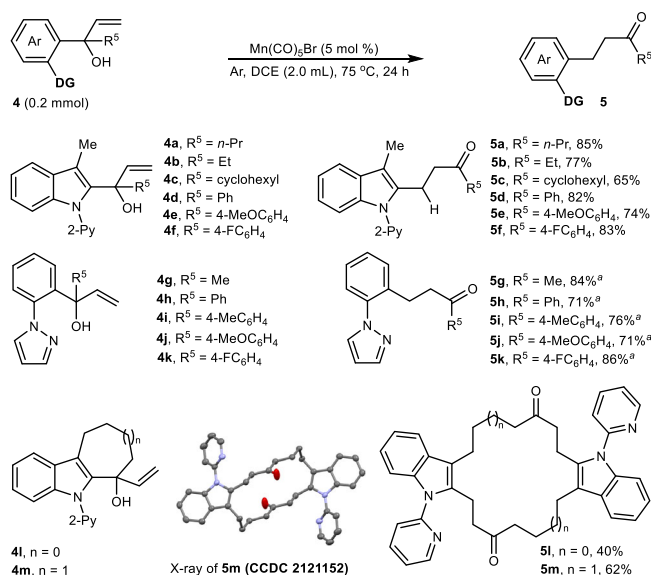


Fig. 3 | Tertiary allylic-alcohol scope. All the reactions were performed in a sealed tube, followed by flash chromatography on SiO₂. The yields were determined by isolation. ^aThe reaction temperature is 100 °C.

80% with excellent chemoselectivity without the formation of **2a** (entries 7–12 vs. 13). Notably, Cp*Co(CO)I₂ and Cp*Rh(CH₃CN)₃(SbF₆)₂ catalysts surveyed under the optimized conditions delivered **3a** with very poor reaction conversions and chemoselectivity (entries 14 and 15).

Substrate scope

With established reaction conditions, the α-(2-indolyl)-substituted secondary allylic alcohols were evaluated by using the optimized conditions. As summarized in Fig. 2, comparison with electroneutral indolyl-substituted allylic-alcohol **1b**, Mn(I)-catalyzed [1,3]-sigmatropic rearrangement of α-[2-(3'-alkylindolyl)] and α-[2-(3'-aryllindolyl)]-substituted allylic alcohols including **1a** and **1c–1e** could efficiently produce 2-carbonylethylindoles **3a–3e** in good to excellent yields (66–80%), regardless of the steric hindrance from C3-substituents of indolyl ring (entry 1). Meanwhile, electron-donating 5-Me, 5-MeO, 5-halo-, and even strong electron-withdrawing 6-CF₃-indole-based allylic alcohols **1f–1j** in which indolyl C3-position kept unsubstituted, could also successfully undergo carbon–carbon activation and 1,3-STR to provide **3f–3j** in 65–73% yields (entry 2). Moreover, *N*-electron-rich and *N*-electron-deficient pyridyl-substituted α-(2-indolyl)alcohols (**1k–1o**) were also well-tolerable in this transformation to assemble β-(2-indolyl)propenals **3k–3o** with good conversions (66–70%) (entry 3). Again, switching terminal allylic alcohols to the internal allylic-alcohol **1p** could still furnish the corresponding rearrangement product **3p** in 62% (entry 4). Of noted, α-(*N*-(2-pyrimidyl)indolyl) allylic-alcohol **1q** and α-(*N*-(2-pyrrolyl)pyrrolyl) allylic-alcohol **1r** also participated in this carbon-skeleton rearrangement, providing **3q** (76%) and **3r** (35%), respectively (entry 5).

In comparison with the photocatalyzed 1,3-alkyl shift of tertiary allylic alcohols reported by Knowles⁵¹, our catalysis system could be applied to α-aryl-tertiary allylic alcohols **4**, which underwent chemoselective 1,3-aryl transposition (Fig. 3). Among them, α-(2-indolyl)-α-alkyl-allylic alcohols (**4a–4c**) and α-(2-indolyl)-α-aryl-allylic alcohols (**4d–4f**) worked well to deliver 2-indolyl-tethered ketones **5a–5f** in 65–85% yields. Moreover, switching α-(2-indolyl)-allylic alcohols to α-phenyl-allylic alcohols (**4g–4k**) in which pyrazole was utilized as a directing group, could also produce the corresponding 2-phenyl-tethered ketones **5g–5k** in excellent reaction conversions (71–86%). Importantly, the potential breadth of the utility of this methodology is further illustrated with different six- and seven-membered α-vinyl cycloalkylalcohols **4l** and **4m**, which are effective substrates for assembling sixteen- and eighteen-membered macrocyclic molecules **5l** (**4l**) and **5m** (**4m**) (40%) and **5m** (62%, CCDC 2121152) via a carbon–carbon σ bond cleavage-based bimolecular [2*n* + 4] coupling-cyclization (see Supplementary Fig. 7 for the possible reaction mechanism of the formation of **5l** and **5m**).

Encouraged by Rh(I)-catalyzed 1,3-alkynyl shift of alkynyl alkenyl carbinols in which Csp³–Csp bond cleavage occurred⁵², we further evaluated the rearrangement reactivity of different α-(2-indolyl) propargyl alcohols (Fig. 4). Interestingly, Mn(I)-catalyzed 1,2-STR of internal propargyl alcohols (**6a–6f**) could occur to produce α-indolyl-α-vinyl aldehydes **7a–7f** in 55–84% yields, and the carbon-skeleton rearrangement model belongs to 1,2-STR instead of 1,3-STR. Among them, the exact structure of **7f** (CCDC 2121154) was determined by its single-crystal X-ray diffraction. However, if terminal propargyl alcohol **6g** was subjected to the same reaction system, the desired 1,3-STR product 3-(2-indolyl)-propargyl aldehyde **7g** (38%) was produced possibly due to the absence of steric hindrance from the terminal substituent of propargyl alcohols. In comparison, switching terminal propargyl alcohol **6g** to the substrate **6h** with a larger size of methyl group at the alkyne terminus produced both 1,2-STR product **7h** (35%) and 1,3-STR product **7h'** (62%, *E/Z* = 1:3.3)⁵³. Again, we explored the reactivity of α-(2-indolyl)-α-alkyl-propargyl alcohols (**6i** and **6j**) and α-(2-indolyl)-α-aryl-propargyl alcohol **6k**, and found these tertiary alcohols still smoothly underwent regioselective 1,2-STR to provide the corresponding α-(2-indolyl)-β-alkyl-α, β-unsaturated ketones **7i** (66%), **7j** (48%) and α-(2-indolyl)-β-phenyl-α, β-unsaturated ketone **7k** (77%), respectively. Similarly, 1-(2-indolyl)-3-phenylpropargyl alcohols with different substituents in the indolyl C-5 position were also amenable to this transformation, producing the desired α-(2-indolyl)-allylic aldehydes **7l–7q** in 38–60% yields, in which the substituents

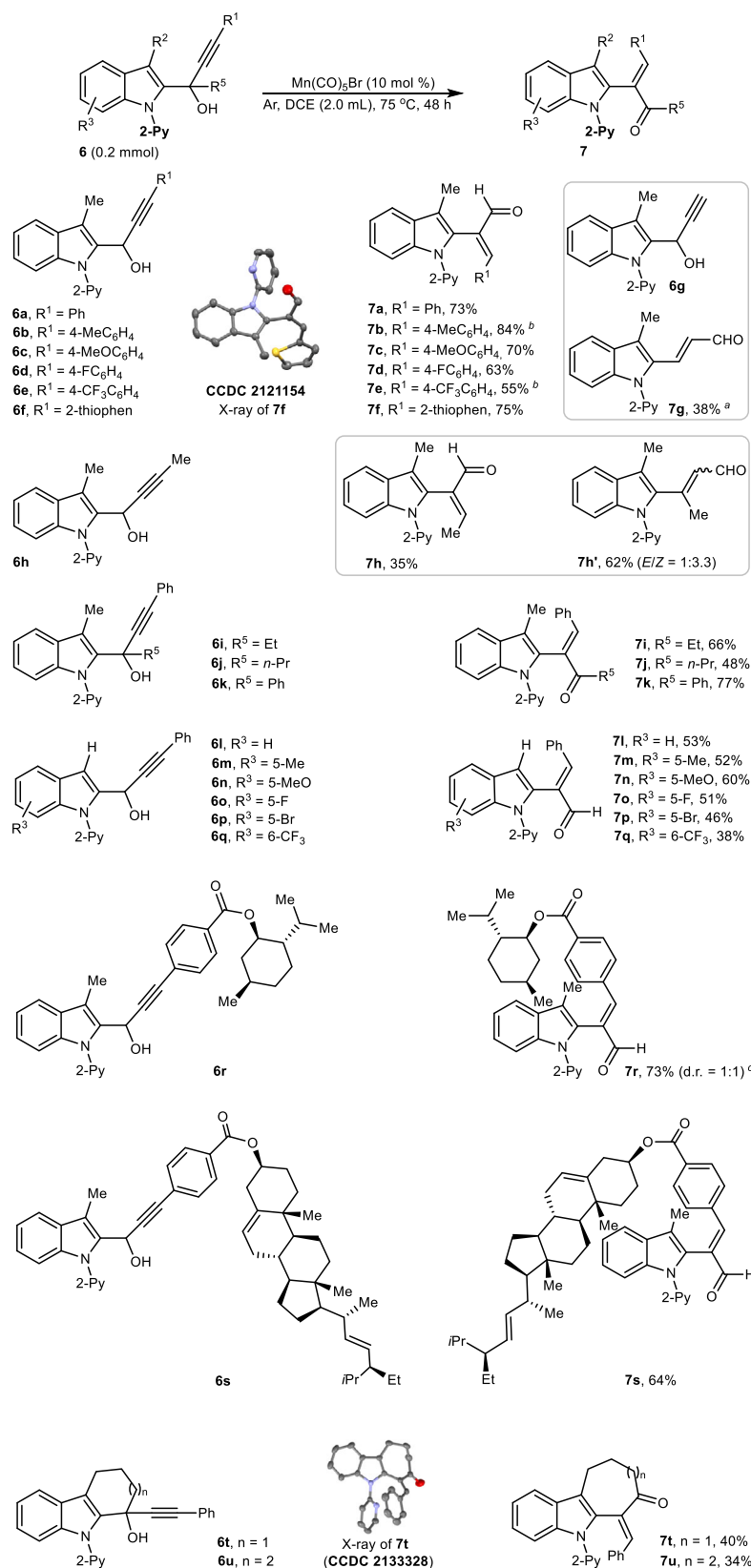


Fig. 4 | Propargylalcohol scope. All were performed in a sealed tube, followed by flash chromatography on SiO_2 . The yields were determined by isolation. ^aThe reaction time is 24 h. ^bThe reaction time is 72 h. ^cDiastereomeric ratio (d.r.) was measured by ^1H NMR spectrum.

including methyl- (**6m**), methoxyl- (**6n**), fluoro- (**6o**), bromo- (**6p**), trifluoromethyl- (**6q**), showed an apparently electronic effect on the carbon-skeleton rearrangement. More complex alkoxy carbonyl phenyl-tethered propargyl alcohols, which were

derived from the natural menthol (**6r**) and stigmasterol (**6s**), could still undergo intramolecular 1,2-STR to deliver the corresponding indole-containing menthol and stigmasterol derivatives **7r** (73%) and **7s** (64%), respectively. Importantly, it should be pointed out that the Mn(I)-

catalyzed 1,2-STR of α -alkynyl cycloalkylalcohols **6t** and **6u** led to a monomolecular $[n+1]$ ring-extension instead of bimolecular $[2n+4]$ coupling-cyclization, furnishing seven-membered 2-benzylidenecycloheptan-1-one **7t** (40%, CCDC 2133328) and eight-membered 2-benzylidenecyclooctan-1-one **7u** (34%), respectively.

Application

To showcase our system's synthetic utility (Fig. 5), the pyrimidyl moiety from aldehydes **3q** could be readily removed to access free (N-H) β -(2-indolyl)ethyl-1,3-dioxolane **8** (75%). Moreover, the indole-derived aldehydes **3a** and **7a** could be further utilized as versatile platform-molecules for diversity-oriented assembly of 4-(2-indolyl)alkyne **9** (71%), 4-(2-indolyl)-5-phenylpenta-2,4-dienitrile **10** (37%) and 2-(2-indolyl)-1,4-diphenylbuta-1,3-diene **11** (67%) by coupling with α -diazophosphonate, acetonitrile and diethyl benzylphosphonate, respectively. Of course, α , β -unsaturated aldehyde **7a** could be regioselectively reduced by NaBH_4 to give 2-(2-indolyl)-3-phenyl-allylic alcohol **13** (82%). Interestingly, the reaction between aldehyde **7a** and Me_3SiOK still provided unexpected 2-phenethyl-indole **12** (44%) through reductive deformylation. Finally, 4-(2-indolyl)pyrazole **14** (42%) was obtained after subjecting **7a** to the coupling-cyclization with phenylhydrazine.

Mechanistic investigations

To gain insights into the mechanism of the Mn(I)-catalyzed sigma-tropic rearrangement, we performed the carbon-skeleton rearrangement of **1a** with D_2O under the standard reaction system, and obtained *d*-**2a** (77%) in which 45% D was incorporated into the α -position of aldehyde (Fig. 6a), indicating that either keto-enol isomerization or protonation of carbon-metal bonds was involved in this transformation (the deuteration of the product **3a** was also performed in the presence of D_2O (5.0 equiv.) under the standard conditions, and 7.5% D was observed at the α -position of aldehyde **3a**, please see SI for more details). Evaluating the reactivity of α -(2-(*N*-phenylindolyl))allylic alcohol **1u** as a substrate only gave an intramolecular cyclization product **3u'** (61%) instead of 1,3-STR product **3u** (Fig. 6b), demonstrating that pyridine played a key chelation-assisted role to enable this carbon-skeleton rearrangement.

Comparison with the reactivity of allylic-alcohol **1a** and 2-unsubstituted *N*-pyridylindole **7** under the same reaction conditions (Fig. 6c vs. 6d), it was found that Mn(I)-catalyzed Csp²-H bond cross-coupling of **7** with acrylaldehyde at 45 °C could only give **3a** with poor conversion (75% vs. 15%). These observations pointed to an understanding mechanism that 2-unsubstituted indole **7** was not a possible reaction intermediate derived from C–C σ bond cleavage of **1a**;

Meanwhile, the subsequent Mn(I)-catalyzed C–H activation and cross-coupling with acrylaldehyde were not possibly involved in this rearrangement. The intermolecular competing reactions between **4a** and **1g** produced 1,3-STR products **5a** (64%), **5n** (31%), **3c** (43%) and **3a** (24%), indicating that cyclomanganated species and the in-situ generated acrylaldehydes probably underwent different site-selective Mn-carbonyl and Mn-alkene complexation via a step-wise process (Fig. 6e).

Based on these control experiments, the possible reaction mechanism is proposed in Fig. 7. The interaction between allylic-alcohol **1a** with $\text{Mn}(\text{CO})_5\text{Br}$ produced cyclomanganated species **A**, followed by chelation-assisted β -aryl elimination to give six-coordination Mn-carbonyl complexes **B**, in which the “carbonyl oxygen” of the in-situ generated acrylaldehyde coordinated to Mn(I) cations. Subsequently, Mn-aldehyde intermediate **B** underwent an intramolecular ligand exchange to give Mn-alkene complexes **C** in Path a. The subsequent migratory insertion and protonation of carbon-Mn bonds of complexes **C** afforded the 1,3-STR product **3a**. Of course, an alternative intramolecular Michael-addition initiated by Mn-aldehyde intermediate **B** via Path b could possibly proceed to furnish enol oxygen-coordinated Mn(I)-complexes **E**, which then underwent a cascade protonation and keto-enol tautomerization to afford **3a**. Instead, indole **7** and Mn-complexes **F** as possible intermediates, were not involved in this [1,3]-sigmatropic rearrangement, supported by our experimental exclusion of the C–H activation (Fig. 6d).

Density functional theory (DFT) studies were performed to explore the Mn(I)-catalyzed carbon-skeleton rearrangement (the potential free energy profiles of the major reaction pathways in Fig. 8 and the full version in Supplementary Fig. 8). The transformation begins with the cyclomanganated complex **A**. Both the *cisoid* and the *transoid* isomers of the formed enal are considered for the β -aryl elimination. The Gibbs free energy of *transoid*-**A** is 2.5 kcal/mol higher than that of *cisoid*-**A** due to the steric effect between the vinyl and the indole fragments. The release of one CO molecule from the cyclomanganated complex **A** gives intermediate **A1** (*cisoid*-**A1**: 9.3 kcal/mol vs. *transoid*-**A1**: 10.6 kcal/mol), providing a vacant site for the β -aryl elimination. The chelation-assisted β -aryl elimination from *cisoid*-**A1** or *transoid*-**A1** then goes through transition states *cisoid*-**TS1** (16.2 kcal/mol) or *transoid*-**TS1** (18.5 kcal/mol), respectively, to furnish the six-coordination Mn-carbonyl intermediates **B** (*cisoid*-**B**: 1.4 kcal/mol vs. *transoid*-**B**: −1.2 kcal/mol). The Gibbs free energy of activation of *cisoid*-**TS1** is slightly lower than that of *transoid*-**TS1** by 2.3 kcal/mol due to the similar steric effect. After C–C sigma bond cleavage, as expected the *transoid* enal *transoid*-**B** (−1.2 kcal/mol) is more stable than the *cisoid* isomer *cisoid*-**B** (1.4 kcal/mol). The Mn-carbonyl intermediates **B** could isomerize to the Mn-alkene intermediates **C**

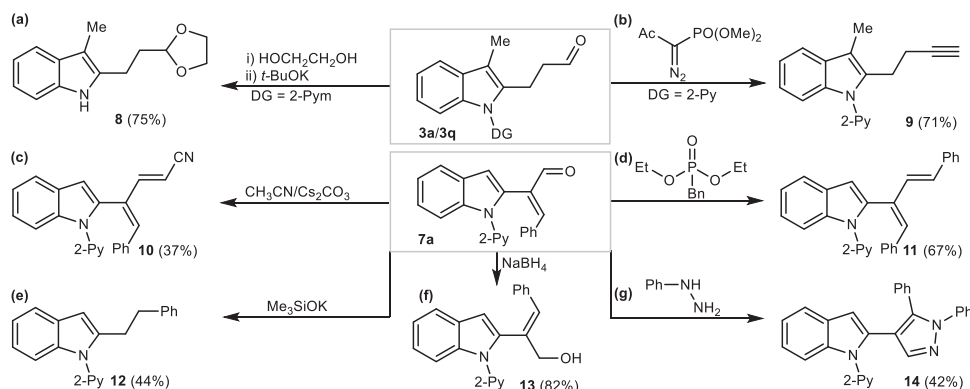


Fig. 5 | Synthetic applications. **a** Removal of pyrimidyl group. **b** Alkynylation of aldehydes. **c** Cyanation of aldehydes. **d** Arylvinylation of aldehydes. **e** Reduction of carbon–carbon double bonds and carbonyl group from α , β -unsaturated

aldehydes. **f** Reduction of aldehydes. **g** Coupling-cyclization of α , β -unsaturated aldehydes with hydrazines.

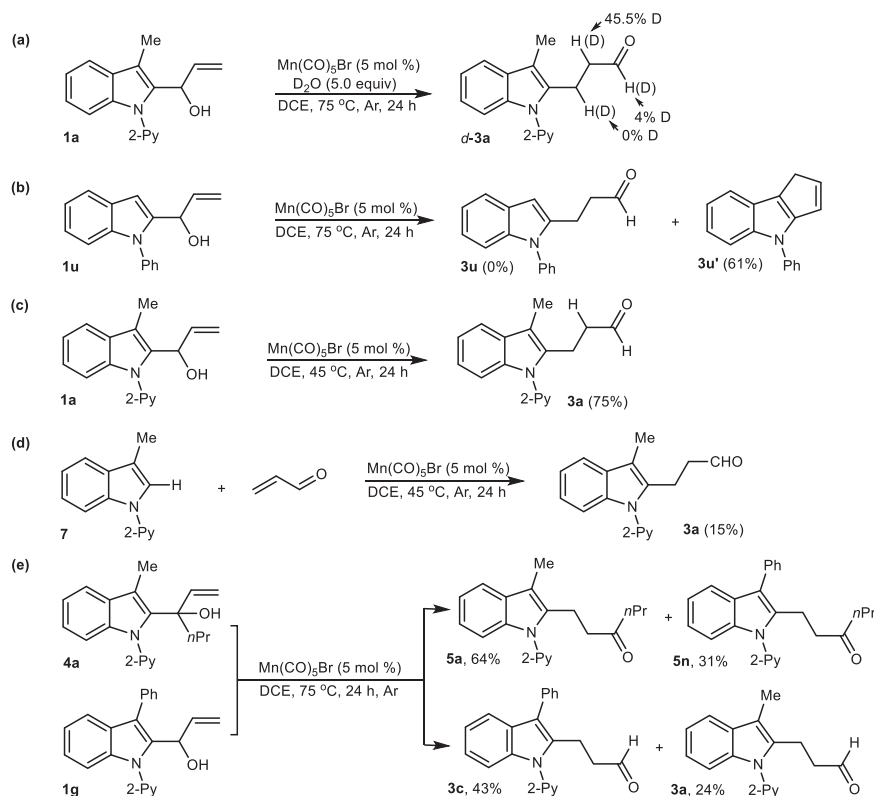


Fig. 6 | Preliminary mechanism studies. a H/D exchange experiment. **b** Intramolecular cyclization of α -[2-(*N*-phenyl) indolyl]allylic-alcohol. **c** Csp^2 - Csp^3 σ bond activation-directed carbonylethylation of indoles. **d** Csp^2 -H bond activation-directed carbonylethylation of indoles. **e** Mn(I)-catalyzed cross-coupling reaction via 1,3-STR.

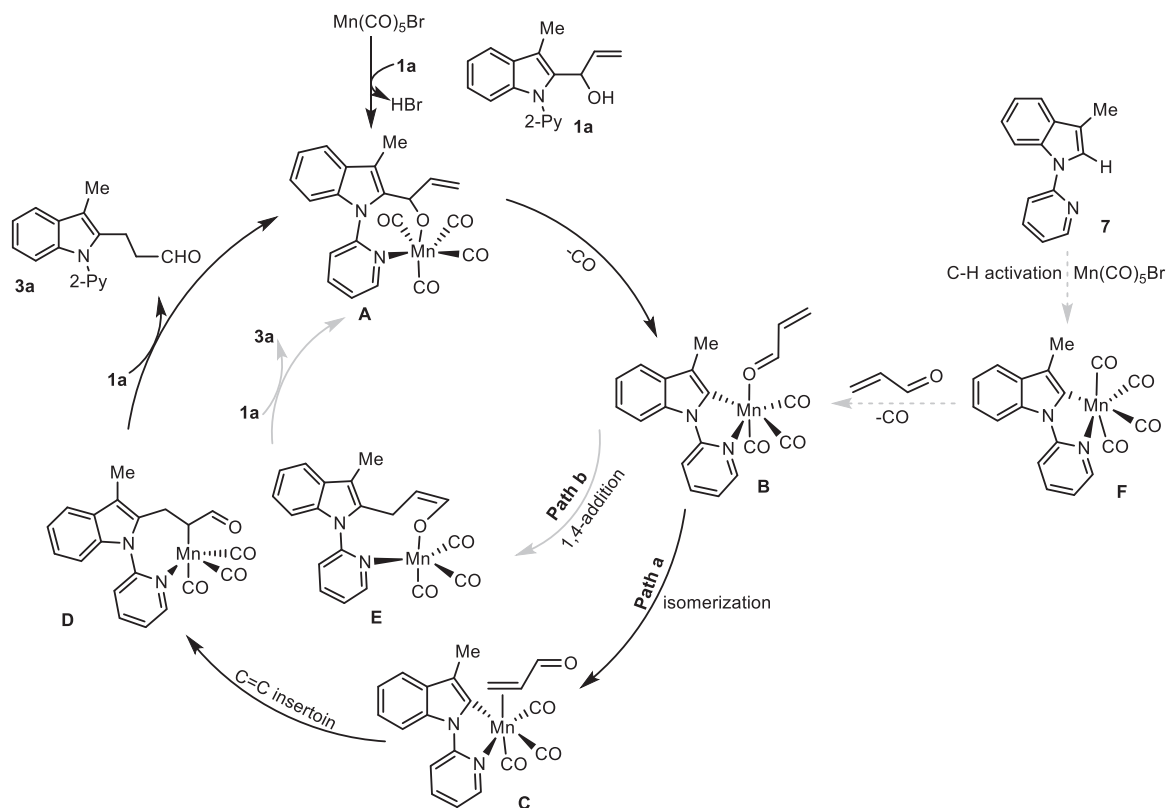


Fig. 7 | Proposed reaction mechanism. Path a Mn(I)-catalyzed 1,3-STR via intramolecular ligand exchange and migratory insertion. **Path b** Mn(I)-catalyzed 1,3-STR via intramolecular Michael-addition.

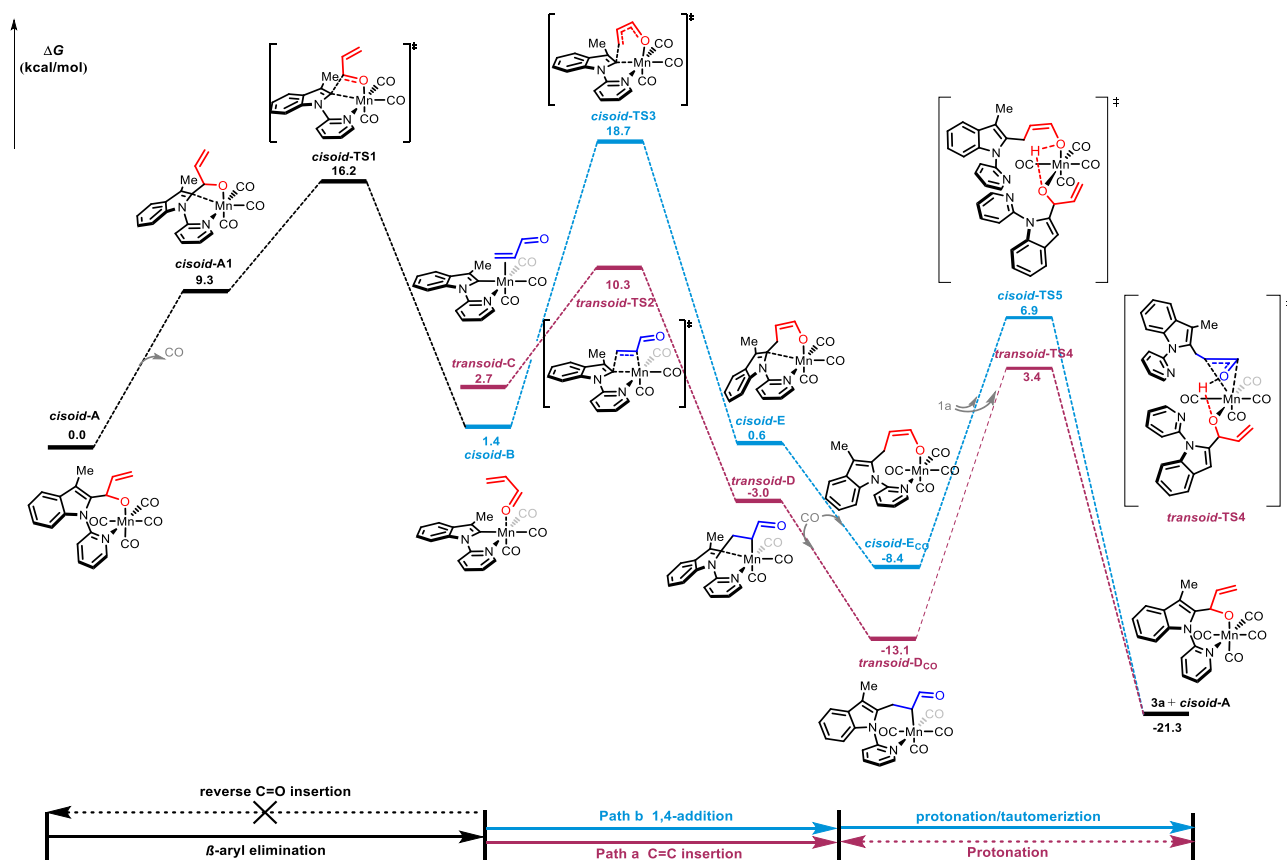


Fig. 8 | Computed potential energy surfaces for the major reaction pathways of the Mn(I)-catalyzed carbon-skeleton rearrangement via C–C bond activation at the SMD(DCE)/M06L/Def2tzvp//M06L/def2svp level of theory. Purple line the

DFT-computed energy surfaces of Path a. Blue line the DFT-computed energy surfaces of Path b.

(*cisoid-C*: 4.8 kcal/mol vs. *transoid-C*: 2.7 kcal/mol). Subsequently, the Mn-alkene intermediate **C** initiates the migratory C=C insertion to afford cyclo Mn-alkyl intermediate **D** through the four-membered ring transition state **TS2** (Path a). Compared with *cisoid-TS2* (11.4 kcal/mol), *transoid-C* isomer results in a more stable migration insertion transition state *transoid-TS2* (10.3 kcal/mol). Nevertheless, the formed Mn-alkyl intermediate **D** will recombine the CO ligand and release product **3a** after proton transfer and keto-enol tautomerism. The OH of **1a** coordinates with the metal center of intermediate **D_{CO}** to promote the intramolecular proton transfer from **1a** to acrylaldehyde via transition states *cisoid-TS4* (4.2 kcal/mol) or *transoid-TS4* (3.4 kcal/mol), which then releases **3a** after keto-enol tautomerism. On the other hand, the Mn-carbonyl **B** promoted 1,4-Michael-addition (Path b) is suggested to be less favored with a calculated Gibbs free energy of 18.7 kcal/mol for transition state *cisoid-TS3* due to the ring constraint. Although 1,4-addition may produce the enolate oxygen-coordinated Mn(I)-intermediates *cisoid-E* (0.6 kcal/mol). Similarly, the introduction of **1a** to *cisoid-E_{CO}* initiates the proton transfer via transition state *cisoid-TS5* (6.9 kcal/mol), leading to **3a** after keto-enol tautomerism.

To further understand the driving force of the Mn(I)-catalyzed sigmatropic rearrangement, the localized Kohn-Sham orbitals and distortion/interaction analysis of the migratory insertion (C=C insertion) and the reverse β -aryl elimination (C=O insertion) were carried out. As shown in Fig. 9, the reverse β -aryl elimination reaction (C=O insertion) is driven by 1) the interaction between the C-Mn p-d orbital and the C=O π^* antibonding orbital, and 2) the interaction between the C=O π orbital and the Mn d_{z^2} antibonding orbital. In comparison, the C=C insertion is contributed by the donation of the C-M p-d orbital to the C=C π^* orbital and the donation of the C=C π orbital to the antibonding d_{z^2} orbital. In both cases, the energy gaps

between the C-M p-d orbital and the π^* orbital (3.10 eV for the C=O insertion, 3.05 eV for the C=C insertion) are smaller than those between the π orbital and the antibonding d_{z^2} orbital (4.46 eV for the C=O insertion, 4.54 eV for the C=C insertion), suggesting the p-d to π^* interaction attributes mainly for the insertion. Notably, the p-d to π^* interaction is more significant in the C=C insertion ($\Delta E_{\text{gap}} = 3.05$ eV) than in the C=O insertion ($\Delta E_{\text{gap}} = 3.10$ eV), resulting in a better interaction energy ($\Delta E_{\text{int}} = -14.3$ kcal/mol) in the C=C insertion transition state *transoid-TS2*, which is probably the driving force of the preference of C=C insertion over C=O insertion for the rearrangement process. Furthermore, the orbital composition analysis in the LUMO of the substrates indicates that the terminal C^4 p orbital (32.9%) in the C=C insertion step is greater than the carbonyl C^2 p orbital (27.5%) in the C=O insertion step, resulting in a large driving force for the C=C insertion, guaranteeing the subsequent 1,3-STR. The difference in the interaction energies between *transoid-TS2* (-14.3 kcal/mol) and *cisoid-TS1* (-7.8 kcal/mol) thus resulted in a lower Gibbs free energy of activation for the C=C insertion transition state *transoid-TS2*.

Discussion

In conclusion, we developed a Mn(I)-catalyzed carbon-skeleton rearrangement via C–C σ bond cleavage. A variety of α -aryl- β , γ -unsaturated alcohols were applicable to this simple catalytic system. This protocol features with [1,*n*]-sigmatropic rearrangement ($n = 2, 3$), leading to 1,2-STR and 1,3-STR to reorganize carbon-skeletons with high atom- and step-economy. This sigmatropic rearrangement strategy can enrich the rearrangement chemistry and enhance the development of more challenging carbon-skeleton rearrangements in the future.

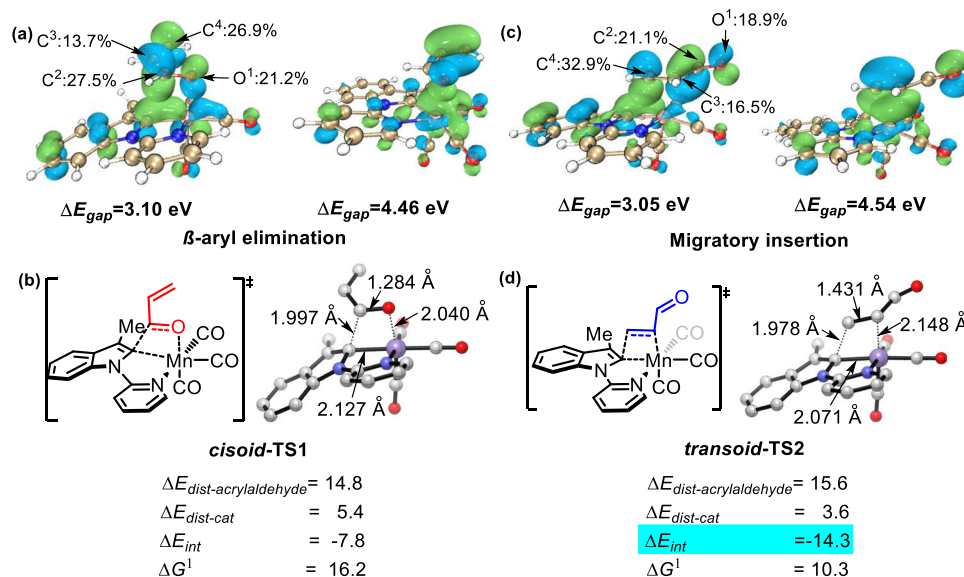


Fig. 9 | The localized Kohn-Sham orbitals and distortion/interaction analysis. **a** C-Mn p-d orbital and C=O π^* antibonding orbital interaction, C=O π orbital and Mn dz^2 orbital interaction. **b** Deformation/interaction analysis of the transition state for the β -aryl elimination pathway. **c** C-M p-d orbital and C=C π^* orbital

interaction, C=C π orbital and Mn dz^2 orbital interaction. **d** Deformation/interaction analysis of the transition state for the migratory insertion pathway. Energies are in kcal/mol, isovalue of Kohn-Sham orbitals is 0.05.

Methods

Procedure for the Mn(I)-catalyzed sigmatropic rearrangement of β , γ -unsaturated alcohols

All the reactions were run in an oven-dried 2 dram vial fitted with an oven-dried Teflon coated stir bar, and a Teflon cap under argon atmosphere. The $Mn(CO)_5Br$ that was used was stored in a freezer. Before every reaction set-up, DCE was freshly distilled. To a 10 mL vial equipped with a magnetic stir bar, was added α -aryl- β , γ -unsaturated alcohols (0.2 mmol), $Mn(CO)_5Br$ (5 mol %) and DCE (2.0 mL) under Ar atmosphere. The reaction mixture was then allowed to stir at 75 °C for 24 h. After the reaction mixture was cooled down, the corresponding reaction mixture was purified by flash chromatography on silica gel to afford the desired 1,2-STR and 1,3-STR products.

Data availability

The authors declare that the data relating to the materials and methods, experimental procedures, mechanism research, NMR spectrum (the original Data-I in supplementary data file), HR-MS spectrum (the original Data-II in supplementary data file), IR spectrum (the original Data-III in supplementary data file), DFT calculations (the original Data-IV in supplementary data file), and X-ray structural analysis (the original Data-V in supplementary data file) are available within its Supplementary Information file, while the original data has been deposited on figshare [<https://figshare.com/s/46dc86c784eb71d8d7c9>]. The X-ray crystallographic coordinates for structures **5m**, **7f** and **7t** reported in this study have been deposited at the Cambridge Crystallographic Data Centre (CCDC) under [CCDC 2121152](#), [CCDC 2121154](#) and [CCDC 2133328](#), respectively. These data can be obtained free of charge from The Cambridge Crystallographic Data Centre via www.ccdc.cam.ac.uk/data-request/cif.

References

1. Friščić, T., Mottillo, C. & Titi, H. M. Mechanochemistry for synthesis. *Angew. Chem. Int.* **59**, 1018–1029 (2020).
2. Takacs, L. The historical development of mechanochemistry. *Chem. Soc. Rev.* **42**, 7649–7659 (2013).
3. Mo, X., Morgan, T. D. R., Ang, H. T. & Hall, D. G. Scope and mechanism of a true organocatalytic beckmann rearrangement with a boronic acid/perfluoropinacol system under ambient conditions. *J. Am. Chem. Soc.* **140**, 5264–5271 (2018).
4. Marthala, V. R. R. et al. Beckmann rearrangement of 15N-cyclohexanone oxime on zeolites silicalite-1, H-ZSM-5, and H-[B] ZSM-5 studied by solid-state NMR spectroscopy. *J. Am. Chem. Soc.* **128**, 14812–14813 (2006).
5. Snape, T. J. Recent advances in the semi-pinacol rearrangement of α -hydroxy epoxides and related compounds. *Chem. Soc. Rev.* **36**, 1823–1842 (2007).
6. Zheng, G., Li, Y., Han, J., Xiong, T. & Zhang, Q. Radical cascade reaction of alkynes with *N*-fluoroarylsulfonimides and alcohols. *Nat. Commun.* **6**, 7011 (2015).
7. Ye, Y. et al. Fungal-derived brevianamide assembly by a stereo-selective semipinacolase. *Nat. Catal.* **3**, 497–506 (2020).
8. Snape, T. J. A truce on the Smiles rearrangement: revisiting an old reaction-the Truce-Smiles rearrangement. *Chem. Soc. Rev.* **37**, 2452–2458 (2008).
9. Holden, C. M. & Greaney, M. F. Modern aspects of the smiles rearrangement. *Chem. Eur. J.* **23**, 8992–9008 (2017).
10. Abrams, R., Jesani, M. H., Browning, A. & Clayden, J. Triarylmethanes and their medium-ring analogues by unactivated truce-smiles rearrangement of benzanilides. *Angew. Chem. Int. Ed.* **60**, 11272–11277 (2021).
11. Yan, J. et al. A radical smiles rearrangement promoted by neutral eosin Y as a direct hydrogen atom transfer photocatalyst. *J. Am. Chem. Soc.* **142**, 11357–11362 (2020).
12. Chen, F. J. et al. Photocatalyzed cycloaromatization of vinylsilanes with arylsulfonyl azides. *Nat. Commun.* **12**, 3304 (2021).
13. Ye, L. W. et al. Nitrene transfer and carbene transfer in gold catalysis. *Chem. Rev.* **121**, 9039–9112 (2021).
14. Yang, Z., Stivanin, M. L., Jurberg, I. D. & Koenigs, R. M. Visible light-promoted reactions with diazo compounds: a mild and practical strategy towards free carbene intermediates. *Chem. Soc. Rev.* **49**, 6833–6847 (2020).
15. Phelps, R. & Orr-Ewing, A. J. Direct observation of ylide and enol intermediates formed in competition with wolff rearrangement of photoexcited ethyl diazoacetate. *J. Am. Chem. Soc.* **142**, 7836–7844 (2020).

16. Wei, Y. et al. Enantioselective trapping of Pd-containing 1, 5-dipoles by photogenerated ketenes: access to 7-membered lactones bearing chiral quaternary stereocenters. *J. Am. Chem. Soc.* **141**, 133–137 (2019).
17. Hu, X. W. et al. Co(III)-catalyzed coupling-cyclization of aryl C-H bonds with α -diazoketones involving Wolff rearrangement. *ACS Catal* **8**, 1308–1312 (2018).
18. Trost, B. M. & Tracy, J. S. Catalytically generated vanadium enolates formed via interruption of the Meyer-Schuster rearrangement as useful reactive intermediates. *Acc. Chem. Res.* **53**, 1568–1579 (2020).
19. Lutz, R. P. Catalysis of the cope and Claisen rearrangements. *Chem. Rev.* **84**, 205–247 (1984).
20. Castro, A. M. M. Claisen rearrangement over the past nine decades. *Chem. Rev.* **104**, 2939–3002 (2004).
21. Gajewski, J. J. The Claisen rearrangement. response to solvents and substituents: the case for both hydrophobic and hydrogen bond acceleration in water and for a variable transition state. *Acc. Chem. Res.* **30**, 219–225 (1997).
22. Rycek, L. & Hudlicky, T. Applications of the Wittig-still rearrangement in organic synthesis. *Angew. Chem., Int. Ed.* **56**, 6022–6066 (2017).
23. Nakai, T. & Tomooka, K. Asymmetric [2, 3]-Wittig rearrangement as a general tool for asymmetric synthesis. *Pure Appl. Chem* **69**, 595–600 (1997).
24. Reisman, S. E., Ready, J. M., Hasuoka, A., Smith, C. J. & Wood, J. L. Total synthesis of (\pm)-Welwitindolinone A isonitrile. *J. Am. Chem. Soc.* **128**, 1448–1449 (2006).
25. Chapman, L. M., Beck, J. C., Wu, L. & Reisman, S. E. Enantioselective total synthesis of (+)-Pisguadial B. *J. Am. Chem. Soc.* **138**, 9803–9806 (2016).
26. Ju, W., Wang, X., Tian, H. & Gui, J. H. Asymmetric total synthesis of clonastatins A and B. *J. Am. Chem. Soc.* **143**, 13016–13021 (2021).
27. Jun, C. H. Transition metal-catalyzed carbon-carbon bond activation. *Chem. Soc. Rev.* **33**, 610–618 (2004).
28. Chen, F., Wang, T. & Jiao, N. Recent advances in transition-metal-catalyzed functionalization of unstrained carbon-carbon bonds. *Chem. Rev.* **114**, 8613–8661 (2014).
29. Nakao, Y. Metal-mediated C-CN bond activation in organic synthesis. *Chem. Rev.* **121**, 327–344 (2021).
30. Gozin, M., Weisman, A., Ben-David, Y. & Milstein, D. Activation of a carbon-carbon bond in solution by transition-metal insertion. *Nature* **364**, 699–701 (1993).
31. Goldman, A. S. Carbon-carbon bonds get a break. *Nature* **463**, 435–436 (2010).
32. Fumagalli, G., Stanton, S. & Bower, J. F. Recent methodologies that exploit C-C single-bond cleavage of strained ring systems by transition metal complexes. *Chem. Rev.* **117**, 9404–9432 (2017).
33. Song, F., Gou, T., Wang, B. Q. & Shi, Z. J. Catalytic activations of unstrained C-C bond involving organometallic intermediates. *Chem. Soc. Rev.* **47**, 7078–7115 (2018).
34. Zhu, J., Wang, J. & Dong, G. Catalytic activation of unstrained C(aryl)-C(aryl) bonds in 2,2'-biphenols. *Nat. Chem.* **11**, 45–51 (2019).
35. Liu, J. et al. From alkylarenes to anilines via site-directed carbon-carbon amination. *Nat. Chem.* **11**, 71–77 (2019).
36. Lei, Z. Q. et al. Group exchange between ketones and carboxylic acids through directing group assisted rh-catalyzed reorganization of carbon skeletons. *J. Am. Chem. Soc.* **137**, 5012–5020 (2015).
37. Hu, X. W. et al. Direct carbon-carbon σ bond amination of unstrained arylalkylketones. *ACS Catal* **10**, 8402–8408 (2020).
38. Zhao, T. T., Xu, W. H., Zheng, Z. J., Xu, P. F. & Wei, H. Directed decarbonylation of unstrained aryl ketones via nickel-catalyzed C-C bond cleavage. *J. Am. Chem. Soc.* **140**, 586–589 (2018).
39. Moselage, M., Li, J., Kramm, F. & Ackermann, L. Ruthenium(II)-catalyzed C-C arylations and alkylations: decarbamoylative C-C functionalizations. *Angew. Chem. Int. Ed.* **56**, 5341–5344 (2017).
40. Onodera, S., Togashi, R., Ishikawa, S., Kochi, T. & Kakiuchi, F. Catalytic, directed C-C bond functionalization of styrenes. *J. Am. Chem. Soc.* **142**, 7345–7349 (2020).
41. Wang, D. & Astruc, D. The recent development of efficient Earth-abundant transition-metal nanocatalysts. *Chem. Soc. Rev.* **46**, 816–854 (2017).
42. Gao, K. & Yoshikai, N. Low-valent cobalt catalysis: new opportunities for C-H functionalization. *Acc. Chem. Res.* **47**, 1208–1219 (2014).
43. Su, B., Cao, Z. C. & Shi, Z. J. Exploration of Earth-abundant Transition Metals (Fe, Co, and Ni) as catalysts in unreactive chemical bond activations. *Acc. Chem. Res.* **48**, 886–896 (2015).
44. Chen, P., Billett, B. A., Tsukamoto, T. & Dong, G. “Cut and Sew” transformations via transition-metal-catalyzed carbon-carbon bond activation. *ACS Catal* **7**, 1340–1360 (2017).
45. Fumagalli, G., Stanton, S. & Bower, J. F. Recent methodologies that exploit C-C single-bond cleavage of strained ring systems by transition metal complexes. *Chem. Rev.* **117**, 9404–9432 (2017).
46. Souillart, L. & Cramer, N. Catalytic C-C bond activations via oxidative addition to transition metals. *Chem. Rev.* **115**, 9410–9464 (2015).
47. Shi, C. Y., Li, L., Kang, W., Zheng, Y. X. & Ye, L. W. Claisen rearrangement triggered by transition metal-catalyzed alkyne alkoxylation. *Coord. Chem. Rev.* **446**, 214131 (2021).
48. Wang, T. & Hashmi, A. S. K. 1, 2-, Migrations onto gold carbene centers. *Chem. Rev.* **121**, 8948–8978 (2021).
49. Hu, Y., Zhou, B. & Wang, C. Y. Inert C-H bond transformations enabled by organometallic manganese catalysis. *Acc. Chem. Res.* **51**, 816–827 (2018).
50. Liu, W. & Ackermann, L. Manganese-catalyzed C-H activation. *ACS Catal* **6**, 3743–3752 (2016).
51. Zhao, K., Seidler, G. & Knowles, R. R. 1,3-alkyl transposition in allylic alcohols enabled by proton-coupled electron transfer. *Angew. Chem., Int. Ed.* **60**, 20190–20195 (2021).
52. Nishimura, T., Katoh, T., Takatsu, K., Shintani, R. & Hayashi, T. Rhodium-catalyzed asymmetric rearrangement of alkynyl alkenyl carbinols: synthetic equivalent to asymmetric conjugate alkynylation of enones. *J. Am. Chem. Soc.* **129**, 14158–14159 (2007).
53. Zhu, Q., Luo, Y., Guo, Y., Zhang, Y. & Tao, Y. Saegusa oxidation of enol ethers at extremely low Pd-catalyst loadings under ligand-free and aqueous conditions: insight into the Pd(II)/Cu(II)-catalyst system. *J. Org. Chem.* **86**, 5463–5476 (2021).

Acknowledgements

The authors thank the National Natural Science Foundation of China (No. 21871097, W. Z.; No. 21973113, Z.-F. K.; No. 22271100, W. Z.), the Key-Area Research and Development Program of Guangdong Province, China (No. 2020B010188001, H.-F. J.), and the Guangdong Basic and Applied Basic Research Foundation (No. 2023A1515010070, W. Z.) for the financial support.

Author contributions

W.Z. directed the research. C.Y. and L.S. performed the experiments. Z.K. directed the DFT calculations. X.Z. performed the computational studies. W.Z. wrote the manuscript. H.J. and Z.K. contributed to discussions. (C.Y. and X.Z.) These two authors contributed equally to this work.

Competing interests

The authors declare no competing interests.

Additional information

Supplementary information The online version contains supplementary material available at <https://doi.org/10.1038/s41467-023-37299-x>.

Correspondence and requests for materials should be addressed to Zhuofeng Ke or Wei Zeng.

Peer review information *Nature Communications* thanks Itaru Nakamura, and the other, anonymous, reviewers for their contribution to the peer review of this work. Peer reviewer reports are available.

Reprints and permissions information is available at <http://www.nature.com/reprints>

Publisher's note Springer Nature remains neutral with regard to jurisdictional claims in published maps and institutional affiliations.

Open Access This article is licensed under a Creative Commons Attribution 4.0 International License, which permits use, sharing, adaptation, distribution and reproduction in any medium or format, as long as you give appropriate credit to the original author(s) and the source, provide a link to the Creative Commons license, and indicate if changes were made. The images or other third party material in this article are included in the article's Creative Commons license, unless indicated otherwise in a credit line to the material. If material is not included in the article's Creative Commons license and your intended use is not permitted by statutory regulation or exceeds the permitted use, you will need to obtain permission directly from the copyright holder. To view a copy of this license, visit <http://creativecommons.org/licenses/by/4.0/>.

© The Author(s) 2023